A Multiple Sensor Fault Diagnosis Scheme for Autonomous Surface Vessels ⋆

Abhishek Dhyani * **Rudy R. Negenborn** * **Vasso Reppa** *

* *Department of Maritime and Transport Technology, Delft University of Technology, The Netherlands*
(e-mails: {a.dhyani-1, r.r.negenborn, v.reppa}@tudelft.nl).

Abstract: Autonomous surface vessels (ASVs) have started to operate in many safety-critical scenarios where rich sensor information is required for situational awareness, environmental perception, motion planning, collision avoidance and navigational control. A timely diagnosis of faulty onboard sensors is therefore essential for ensuring maritime safety and reliability. In this paper, a model-based fault diagnosis scheme is presented for ASVs affected by multiple sensor faults. Various monitoring modules comprising nonlinear observers are employed for the detection of faults occurring in the vessel's navigational sensors. Further, multiple fault isolation is performed based on a combinatorial decision logic, achieved by grouping the available sensors into multiple sensor sets. The efficacy of the proposed scheme is illustrated through a simulation example of a vessel trajectory tracking scenario. It demonstrates the scheme's ability to effectively isolate multiple fault combinations impacting the sensors considered.

Keywords: Fault detection and diagnosis, FDI for nonlinear systems, Sensor faults, Safety of marine systems, Autonomous surface vehicles.

1. INTRODUCTION

Autonomous surface vessels (ASVs) will extensively rely on sensors for navigating through open sea and inland waterways. While autonomous navigation with less crew onboard promises improved safety levels, at the same time, a fault in one or more navigational sensors may have serious consequences, such as damage to the vessel, infrastructure, or a human injury. Therefore, it is crucial to diagnose sensor faults quickly and precisely. The diagnostic results can facilitate prompt remedial measures, such as utilizing sensor redundancy or selecting a fault-tolerant control mode, thereby ensuring that the ongoing operation continues with minimum disruptions.

The prevailing approaches for model-based fault detection and isolation (FDI) involve the utilization of observers to generate residual signals. For ASVs, a number of FDI and fault-tolerant control (FTC) methods focusing on actuator faults have been proposed, see for example, Wang et al. (2020); Park and Yoo (2016); Lin et al. (2018). However, it is equally crucial to tackle the sensor FDI problem owing to the large number of sensors installed to enable perception, situational awareness, state (e.g. position, velocity) estimation, etc. Furthermore, the harsh marine environment can potentially contribute to sensor degradation, for example, due to salt spray and moisture (Liu et al. (2016)). Zhang et al. (2021) proposed a nonlinear observer for sensor fault estimation, which is subsequently employed in designing a fault-tolerant model reference reinforcement learning control scheme to guarantee stable tracking for ASVs. The proposed scheme assumes the occurrence of a single fault and therefore may not be suitable for isolating multiple sensor faults. In the work of Blanke (2006), structural analysis is performed to exploit the analytical redundancy of sensors for fault diagnosis, accompanied by a fault-tolerant fusion of sensor data. Rogne et al. (2014) proposed a scheme for the FDI of navigational sensors using a nonlinear observer in conjunction with a "reliable" inertial measurement unit (IMU) sensor. A limitation of the schemes proposed in Blanke (2006); Rogne et al. (2014) is that the effects of external disturbances such as wind force on vessel kinetics are not considered. Wind forces represent the dominant external force in ports and inland waterways (Kepaptsoglou et al. (2015)) and may lead to erroneous fault diagnosis if neglected. Likewise, sensor noise is not taken into account, which could also substantially impact the diagnosis performance.

This paper proposes a nonlinear observer-based sensor FDI scheme for ASVs. The proposed scheme is designed to diagnose multiple faults affecting an ASV's navigational sensors. The ASV is modeled by a 3 degrees of freedom (DOF) hydrodynamic model while considering the influence of sensor noise and wind forces acting on the vessel. The main contributions of this work are two-fold. Firstly, the current body of work has either focused on diagnosing a single fault or multiple faults while only considering the structural or kinematic models. On the other hand, the proposed FDI scheme can diagnose faults affecting

⋆ The research leading to these results has received funding from the European Union's Horizon 2020 research and innovation programme under the Marie Skłodowska-Curie grant agreement No 955768 (MSCA-ETN AUTOBarge) and grant agreement No. 101096923 (SEAMLESS Project). This publication reflects only the authors' view, exempting the European Union and the granting authority from any liability. Project websites:http://etn-autobarge.eu/, https://www.seamless-project.eu/. This research is also supported by the ResearchLab Autonomous Shipping (RAS) of TU Delft.

multiple navigational sensors of an ASV using a detailed kinetic model of the vessel. Secondly, we derive adaptive thresholds for bounding the residuals generated in each FDI monitoring module. Unlike fault detection schemes based on a constant threshold, adaptive thresholds are robust against noise and external disturbances affecting a vessel, such as wind, thereby guaranteeing that no false alarms occur. To the best of author's knowledge, no existing scheme considers adaptive thresholds for the diagnosis of an ASV's navigational sensor faults.

The remainder of this paper is organized as follows: In section 2, the model-based sensor FDI problem for an ASV is formulated. The proposed sensor FDI method is described in section 3. The proposed technique is verified in section 4 by a simulation study involving a model vessel tracking a desired trajectory, and the conclusions are reported in the section 5.

2. PROBLEM FORMULATION

For motion in the horizontal plane, a 3-DOF hydrodynamic model of a vessel is employed and can be described by the following equations (Fossen (2011)):

$$\begin{aligned} \dot{\eta} &= R(\psi)\nu, \\ M\dot{\nu} + C(\nu)\nu + D(\nu)\nu &= \tau + \tau_e. \end{aligned} \tag{1}$$

where, $\eta = [x\ y\ \psi]^T$ is the generalised coordinate vector with x, y denoting the position coordinates and ψ denoting the heading angle; $\nu = [u\ v\ r]^T$ is the generalised velocity vector, with u, v denoting the linear velocities in surge and sway, and r denoting the angular velocity (yaw rate). The variable $\tau = [\tau_u\ \tau_v\ \tau_r]^T$ represents the controlled input force vector and $\tau_e \in \mathbb{R}^3$ is the added force vector, such that $\tau_e = \tau_w + \tau_d$, where τ_w is the force acting on the vessel due to wind and τ_d is an unknown force acting on the vessel resulting from various other external factors such as currents, force applied through a towing system, etc. The terms $M, C(\nu), D(\nu)$ and $R(\psi)$ are the inertia, Coriolis-centripetal, damping, and rotation matrices, respectively, of 3×3 dimensions, with $R(\psi) = \begin{bmatrix} \cos(\psi) & -\sin(\psi) & 0 \\ \sin(\psi) & \cos(\psi) & 0 \\ 0 & 0 & 1 \end{bmatrix}$. Further, $\gamma = \begin{bmatrix} R(\psi)\nu \\ M^{-1}(-C(\nu)\nu - D(\nu)\nu + \tau) \end{bmatrix}$ is used to denote the known nonlinear terms constituting the vessel dynamics. Under the assumption that the ship is symmetrical with respect to the xz and yz planes, the effect of wind on the vessel can be expressed by using the model provided in Fossen (2011). The wind speed $V \in \mathbb{R}$ and direction $\beta_V \in \mathbb{R}$ can be measured in real-time by an anemometer and a weather vane, respectively. For the vessel's localisation, on-board GPS/GNSS, gyrocompass, and accelerometers are favourable due to their small size, low cost, and low energy consumption (Liu et al. (2016)). A GPS/GNSS sensor determines the vessel's position $p = [x\ y]^T$, whereas a gyrocompass and an accelerometer provide the heading (ψ) measurements and the velocity (ν) measurements, respectively. Often the gyrocompass and accelerometer sensors are a part of a 3-axis inertial measurement unit. The sensor's output can be described by

$$\begin{aligned} S_p &: y_p = p + n_p + f_p, \\ S_\psi &: y_\psi = \psi + n_\psi + f_\psi, \\ S_\nu &: y_\nu = \nu + n_\nu + f_\nu, \end{aligned} \tag{2}$$

where, $y_p \in \mathbb{R}^2, y_\psi \in \mathbb{R}$, and $y_\nu \in \mathbb{R}^3$. The terms n and f are vectors denoting the noise and fault affecting the sensor measurements, respectively.

3. NAVIGATIONAL SENSOR FAULT DETECTION AND ISOLATION

This section provides a detailed description of the design of the proposed FDI scheme. The available sensors are decomposed into N sensor sets $\mathcal{S}^{(I)}, I = 1, \ldots, N$, facilitating the isolation of multiple sensor faults. For each sensor set, a corresponding monitoring module composed of various nonlinear observers is used to estimate the sensor measurements. Based on a set of analytical redundancy relations (ARRs), each monitoring module can detect the occurrence of faults. As shown in the Figure 1, each monitoring module $\mathcal{M}^{(I)}$ consists of observers denoted by $\mathcal{O}^{(I)}$, that are used to generate the residual signals. To improve the fault isolability, the residuals must be selectively sensitive to a subset of possible sensor faults. This is achieved by structuring the observers such that each observer recieves as input a subset of the available sensor measurements. The ARRs and subsequently the decisions $D^{(I)}$ are computed by the fault detector submodules. To obtain the ARRs, adaptive thresholds are derived that take into account sensor noise as well as disturbances due to wind and other external factors. Finally, the resulting decisions related to the violation of the ARRs are provided to the aggregator module $\mathcal{A}$, for computing the set of possibly occurring (multiple) fault(s) D_s, and isolating the faulty sensors.

In this work, $N = 2$, and the decomposition is performed such that the monitoring modules are responsible for (a) GPS/GNSS and Gyroscope, (b) Gyroscope and accelerometer sensors, respectively, i.e.,

$$\begin{aligned} S^{(1)} &= \{S^{(1,1)}, S^{(1,2)}\} = \{S_p, S_\psi\}, \\ S^{(2)} &= \{S^{(2,1)}, S^{(2,2)}\} = \{S_\psi, S_\nu\}. \end{aligned} \tag{3}$$

Such a decomposition facilitates the design of the observers in the corresponding monitoring modules in a way that selective sensitivity to the faults is improved. This is further reflected in the resulting theoretical sensor fault patterns, and ultimately leads to an improved sensor fault isolation capability. The corresponding monitoring modules are given by $\mathcal{M}^{(1)}$ and $\mathcal{M}^{(2)}$, respectively.

3.1 Observer design

Sensor FDI is performed by a bank of nonlinear observers, designed to have structured sensitivity to the set of possible faults. For $\mathcal{M}^{(1)}$, being the monitoring module for the GPS/GNSS and gyroscope sensors, the observer dynamics are described by

$$\mathcal{O}^{(1)} : \begin{cases} \dot{\hat{\eta}}^{(1)} = & R(\hat{\psi}^{(1)})\hat{\nu}^{(1)} + K_1\tilde{\eta}^{(1)}, \\ \dot{\hat{\nu}}^{(1)} = & M^{-1}(-C(\hat{\nu}^{(1)})\hat{\nu}^{(1)} - D(\hat{\nu}^{(1)})\hat{\nu}^{(1)} \\ & + \tau) + K_2 R^T(\hat{\psi}^{(1)})\tilde{\eta}^{(1)}, \end{cases} \tag{4}$$

where, $\hat{\eta}^{(1)}$, $\hat{\nu}^{(1)}$ and $\hat{\psi}^{(1)}$ denote the estimations of $\eta = [p\ \psi]^T$, ν and ψ, respectively, and $\tilde{\eta}^{(1)} = y_\eta - \hat{\eta}^{(1)}$,

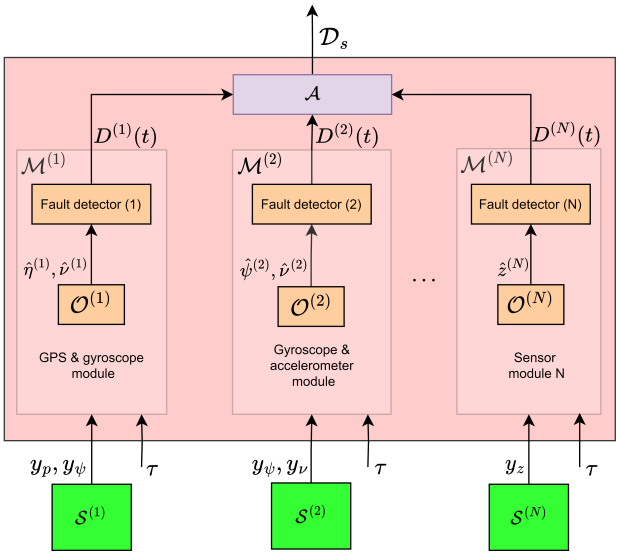

Fig. 1. Proposed architecture of the sensor fault detection and isolation scheme

where $y_\eta = [y_p \ y_\psi]^T$. The gains K_1 and $K_2 \in \mathbb{R}^{3\times3}$ are diagonal matrices. For $\mathcal{M}^{(2)}$, being the monitoring module for the gyroscope and accelerometer sensors, the observer dynamics are described by

$$\mathcal{O}^{(2)}: \begin{cases} \dot{\hat{\psi}}^{(2)} = \hat{r}^{(2)} + K_3\tilde{\psi}^{(2)}, \\ \dot{\hat{\nu}}^{(2)} = M^{-1}(-C(\hat{\nu}^{(2)})\hat{\nu}^{(2)} - D(\hat{\nu}^{(2)})\hat{\nu}^{(2)} \\ \qquad + \tau) + K_4\tilde{\nu}^{(2)}, \end{cases} \tag{5}$$

where, $\tilde{\psi}^{(2)} = y_\psi - \hat{\psi}^{(2)}$ and $\tilde{\nu}^{(2)} = y_\nu - \hat{\nu}^{(2)}$ are the output estimation errors for ψ and ν, respectively. Here, $K_3 \in \mathbb{R}$, and $K_4 \in \mathbb{R}^{3\times3}$ is a diagonal gain matrix.

3.2 Residual generation and adaptive threshold computation

Let us define $z^{(I)}, I = 1, 2$, to be vectors consisting of the vessel states such that $z^{(1)} = [p \ \psi \ \nu]^T$ and $z^{(2)} = [\psi \ \nu]^T$. The residual vector $\varepsilon_{y_z}^{(I)} \in \mathbb{R}^{N_I}$ is defined by

$$\varepsilon_{y_z}^{(I)} = y_z^{(I)} - \hat{z}^{(I)}, \tag{6}$$

where, $y_z^{(I)}$ and $\hat{z}^{(I)}$ represent the measurements and estimations of the vectors $z^{(I)}$ in the $I-$th monitoring module, respectively. The superscript $\{.\}^{(j)}$ will be used to signify that the residual corresponds to the $j-$th sensor, $j \in \{1, \ldots, m_I\}$. In this work, $m_1 = 2$ for $\mathcal{M}^{(1)}$ and $m_2 = 2$ for $\mathcal{M}^{(2)}$, respectively. As a result,

$$\begin{aligned} \varepsilon_{y_z}^{(1)} &= \begin{bmatrix} \varepsilon_{y_z}^{(1,1)} \\ \varepsilon_{y_z}^{(1,2)} \end{bmatrix} = \begin{bmatrix} y_p \\ y_\psi \end{bmatrix} - \begin{bmatrix} \hat{z}^{(1,1)} \\ \hat{z}^{(1,2)} \end{bmatrix}, \\ \varepsilon_{y_z}^{(2)} &= \begin{bmatrix} \varepsilon_{y_z}^{(2,1)} \\ \varepsilon_{y_z}^{(2,2)} \end{bmatrix} = \begin{bmatrix} y_\psi \\ y_\nu \end{bmatrix} - \begin{bmatrix} \hat{z}^{(2,1)} \\ \hat{z}^{(2,2)} \end{bmatrix}, \end{aligned} \tag{7}$$

where, $\left[\hat{z}^{(1,1)} \ \hat{z}^{(1,2)}\right]^T = \left[\hat{p} \ \hat{\psi}\right]^T$ and $\left[\hat{z}^{(2,1)} \ \hat{z}^{(2,2)}\right]^T = \left[\hat{\psi} \ \hat{\nu}\right]^T$ are generated by the observers $\mathcal{O}^{(1)}$, $\mathcal{O}^{(2)}$, respectively. Further, the $j-$th adaptive threshold is defined by $\bar{\varepsilon}_{y_z}^{(I,j)}$, for $I \in \{1, 2\}$ and $j \in \{1, \ldots, m_I\}$, respectively. Under healthy conditions (i.e., no sensor fault), it is denoted by $\bar{\varepsilon}_{y_zH}^{(I,j)}$ and must be computed such that

$$\begin{bmatrix} |\varepsilon_{y_zH}^{(1,1)}| \\ |\varepsilon_{y_zH}^{(1,2)}| \end{bmatrix} \leq \begin{bmatrix} \bar{\varepsilon}_{y_zH}^{(1,1)} \\ \bar{\varepsilon}_{y_zH}^{(1,2)} \end{bmatrix}, \begin{bmatrix} |\varepsilon_{y_zH}^{(2,1)}| \\ |\varepsilon_{y_zH}^{(2,2)}| \end{bmatrix} \leq \begin{bmatrix} \bar{\varepsilon}_{y_zH}^{(2,1)} \\ \bar{\varepsilon}_{y_zH}^{(2,2)} \end{bmatrix}, \tag{8}$$

where, $\varepsilon_{y_zH}^{(I,j)}$ are the residual components under healthy conditions. To carry out this computation, $\varepsilon_{y_zH}^{(I,j)}$ can be expressed in terms of the state estimation error under healthy conditions $\varepsilon_{zH}^{(I,j)}$ as $\varepsilon_{y_zH}^{(I,j)} = \varepsilon_{zH}^{(I,j)} + n_z^{(I,j)}$, with, $\varepsilon_{zH}^{(I,j)} = z^{(j)} - \hat{z}_H^{(I,j)}$. To ensure the convergence of the residual signals under healthy conditions, the following assumptions regarding the vessel dynamics and sensor noise are considered:

Assumption 1. The states $g = [\eta \ \nu]^T$ and the input force τ remain bounded before and after the occurrence of multiple sensor faults, i.e., there exist some compact stability regions $\mathcal{R}^g \subset \mathbb{R}^6$ and $\mathcal{R}^\tau \subset \mathbb{R}^3$ such that $(g, \tau) \in (\mathcal{R}^g \times \mathcal{R}^\tau)$, for all $t \geq 0$.

Assumption 2. The unknown noise affecting the $j-$th sensor $(n_z^{(I,j)})$ is uniformly bounded, i.e., $|n_{z_k}^{(I,j)}| \leq \bar{n}_{z_k}^{(I,j)}$, for all k elements of $n_z^{(I,j)}$, with $\bar{n}_{z_k}^{(I,j)}$ representing a known bound.

Based on these assumptions, the magnitudes of the residual components are bounded by

$$\begin{aligned} \begin{bmatrix} |\varepsilon_{y_zH}^{(1,1)}| \\ |\varepsilon_{y_zH}^{(1,2)}| \end{bmatrix} &\leq \begin{bmatrix} |\varepsilon_{zH}^{(1,1)}| \\ |\varepsilon_{zH}^{(1,2)}| \end{bmatrix} + \begin{bmatrix} \bar{n}_z^{(1,1)} \\ \bar{n}_z^{(1,2)} \end{bmatrix}, \\ \begin{bmatrix} |\varepsilon_{y_zH}^{(2,1)}| \\ |\varepsilon_{y_zH}^{(2,2)}| \end{bmatrix} &\leq \begin{bmatrix} |\varepsilon_{zH}^{(2,1)}| \\ |\varepsilon_{zH}^{(2,2)}| \end{bmatrix} + \begin{bmatrix} \bar{n}_z^{(2,1)} \\ \bar{n}_z^{(2,2)} \end{bmatrix}, \end{aligned} \tag{9}$$

where, $\left[|\varepsilon_{zH}^{(1,1)}| \ |\varepsilon_{zH}^{(1,2)}|\right]^T$ and $\left[|\varepsilon_{zH}^{(2,1)}| \ |\varepsilon_{zH}^{(2,2)}|\right]^T$ are the estimation error magnitudes for the states in the vectors $z^{(1)}$ and $z^{(2)}$, respectively. Further, the dynamics governing the state estimation error of the observer $\mathcal{O}^{(1)}$, can be described by

$$\begin{aligned} \dot{\varepsilon}_{zH}^{(1)} &= \begin{bmatrix} \dot{\varepsilon}_{zH}^{(1,1)} \\ \dot{\varepsilon}_{zH}^{(1,2)} \\ \dot{\varepsilon}_{zH}^{(1,3)} \end{bmatrix} = \begin{bmatrix} -K_{11} & \mathbf{0} & \mathbf{0} \\ \mathbf{0} & -K_{12} & \mathbf{0} \\ \mathbf{0} & \mathbf{0} & -K_2 \end{bmatrix} \begin{bmatrix} \varepsilon_{zH}^{(1,1)} \\ \varepsilon_{zH}^{(1,2)} \\ \varepsilon_{zH}^{(1,3)} \end{bmatrix} + \begin{bmatrix} \tilde{\gamma}_{1H}^{(1)} \\ \tilde{\gamma}_{2H}^{(1)} \end{bmatrix} \\ &+ \begin{bmatrix} \mathbf{0} \\ M^{-1}\tau_e + K_2\nu \end{bmatrix} + \begin{bmatrix} -K_{11} & \mathbf{0} & \mathbf{0} \\ \mathbf{0} & -K_{12} & \mathbf{0} \\ \mathbf{0} & \mathbf{0} & -K_2 \end{bmatrix} \begin{bmatrix} n_z^{(1,1)} \\ n_z^{(1,2)} \\ R^T(\hat{\psi}_H^{(1)})y_\eta \end{bmatrix}, \end{aligned} \tag{10}$$

where, $K_1 = \text{diag}([K_{11} \ K_{12}])$, $\tilde{\gamma}_{1H}^{(1)} = R(\psi)\nu - R(\hat{\psi}_H^{(1)})\hat{\nu}_H^{(1)}$, $\tilde{\gamma}_{2H}^{(1)} = M^{-1}(-C(\nu)\nu - D(\nu)\nu + C(\hat{\nu}_H^{(1)})\hat{\nu}_H^{(1)} + D(\hat{\nu}_H^{(1)})\hat{\nu}_H^{(1)})$, and $\mathbf{0}$ denotes a matrix/vector of zeroes, having a suitable dimension. Solving (10) results in

$$\begin{aligned} \varepsilon_{zH}^{(1)} &= \begin{bmatrix} \varepsilon_{zH}^{(1,1)} \\ \varepsilon_{zH}^{(1,2)} \\ \varepsilon_{zH}^{(1,3)} \end{bmatrix} = \begin{bmatrix} e^{-K_1 t} & \mathbf{0} \\ \mathbf{0} & e^{-K_2 t} \end{bmatrix} \begin{bmatrix} \varepsilon_{zH}^{(1,1)}(0) \\ \varepsilon_{zH}^{(1,2)}(0) \\ \varepsilon_{zH}^{(1,3)}(0) \end{bmatrix} \\ &+ \int_0^t \begin{bmatrix} e^{-K_1(t-\mathfrak{t})} & \mathbf{0} \\ \mathbf{0} & e^{-K_2(t-\mathfrak{t})} \end{bmatrix} \left(\begin{bmatrix} \tilde{\gamma}_{1H}^{(1)}(\mathfrak{t}) \\ \tilde{\gamma}_{2H}^{(1)}(\mathfrak{t}) + M^{-1}\tau_e \end{bmatrix} \right. \\ &\left. + \begin{bmatrix} -K_1 n_\eta \\ -K_2 R^T(\hat{\psi}_H^{(1)}(\mathfrak{t}))n_\eta + K_2(\nu(\mathfrak{t}) - R^T(\hat{\psi}_H^{(1)}(\mathfrak{t}))\eta(\mathfrak{t})) \end{bmatrix} \right) d\mathfrak{t}, \end{aligned} \tag{11}$$

where, $n_\eta = \left[n_z^{(1,1)} \ n_z^{(1,2)}\right]^T$. A bound on $|\varepsilon_{zH}^{(1)}|$ satisfies the inequality

$$|\varepsilon_{zH}^{(1)}| \leq \begin{bmatrix} |e^{-K_1 t}| & \mathbf{0} \\ \mathbf{0} & |e^{-K_2 t}| \end{bmatrix} \begin{bmatrix} |\varepsilon_{zH}^{(1,1)}(0)| \\ |\varepsilon_{zH}^{(1,2)}(0)| \\ |\varepsilon_{zH}^{(1,3)}(0)| \end{bmatrix} + \int_0^t \Bigg(\begin{bmatrix} |e^{-K_1(t-\mathfrak{t})}| & \mathbf{0} \\ \mathbf{0} & |e^{-K_2(t-\mathfrak{t})}| \end{bmatrix} \begin{bmatrix} |\tilde{\gamma}_{1H}^{(1)}(\mathfrak{t})| \\ |\tilde{\gamma}_{2H}^{(1)}(\mathfrak{t})| + |M^{-1}\tau_e| + \\ | - K_2 R^T(\hat{\psi}_H^{(1)}(\mathfrak{t}))n_\eta| + | - K_2(R^T(\hat{\psi}_H^{(1)}(\mathfrak{t}))\eta(\mathfrak{t}) - \nu(\mathfrak{t}))| \end{bmatrix} + \begin{bmatrix} | - K_1 e^{-K_1(t-\mathfrak{t})}| & \mathbf{0} \\ \mathbf{0} & | - K_2 e^{-K_2(t-\mathfrak{t})}| \end{bmatrix} \begin{bmatrix} |n_\eta| \\ \mathbf{0} \end{bmatrix} \Bigg) d\mathfrak{t}. \tag{12}$$

To determine the adaptive thresholds, the following assumptions regarding the system uncertainties are made:

Assumption 3. The following holds for these nonlinear terms representing the system dynamics: (a) γ is Lipschitz in the state $g \in \mathcal{R}^g$ for all $\tau \in \mathcal{R}^\tau$ and $t \geq 0$, (b) τ_w is Lipschitz in $g \in \mathcal{R}^g$ for all $w = [V \ \beta_V]^T \in \mathcal{R}^2$ and $t \geq 0$, where $\mathcal{R}^2 \subset \mathbb{R}^2$ denotes a compact region of stability.

Assumption 4. The unknown force vector τ_d is uniformly bounded, i.e., $|\tau_{d_i}| \leq \bar{\tau}_{d_i}$, where $i \in \{1,2,3\}$ represent the elements of τ_d and $\bar{\tau}_{d_i}$ represents a known bound.

Based on these assumptions, a bound on each term constituting the inequality (12) is determined and is given by

12a. $\left[|\varepsilon_{zH}^{(1,1)}(0)| \ |\varepsilon_{zH}^{(1,2)}(0)| \ |\varepsilon_{zH}^{(1,3)}(0)|\right]^T = \left[\bar{p}^{(1)} \ \bar{\psi}^{(1)} \ \bar{\nu}^{(1)}\right]^T = \bar{z}^{(1)T}$,

12b. $\begin{bmatrix} |e^{-K_1 t}| & \mathbf{0} \\ \mathbf{0} & |e^{-K_2 t}| \end{bmatrix} \leq \rho^{(1)} e^{-\xi^{(1)} t} = \Phi^{(1)}(t)$,

12c. $\begin{bmatrix} | - K_1 e^{-K_1 t}| & \mathbf{0} \\ \mathbf{0} & | - K_2 e^{-K_2 t}| \end{bmatrix} \leq \rho_d^{(1)} e^{-\xi_d^{(1)} t}$,

12d. $|n_\eta| \leq \left[\bar{n}_z^{(1,1)} \ \bar{n}_z^{(1,2)}\right]^T$,

12e. $|\tilde{\gamma}_{1H}^{(1)}| = |R(\psi)\nu - R(\hat{\psi}_H^{(1)})\hat{\nu}_H^{(1)}| \leq \lambda_{\gamma_1^{(1)}} \left[|\varepsilon_{zH}^{(1,1)}| \ |\varepsilon_{zH}^{(1,2)}|\right]^T$,
$|\tilde{\gamma}_{2H}^{(1)}| = |M^{-1}(-C(\nu)\nu - D(\nu)\nu + C(\hat{\nu}_H^{(1)})\hat{\nu}_H^{(1)} + D(\hat{\nu}_H^{(1)})\hat{\nu}_H^{(1)})| \leq \lambda_{\gamma_2^{(1)}} |\varepsilon_{zH}^{(1,3)}|, |M^{-1}\tau_e| \leq \bar{\tau}_e$, and,

12f. $| - K_2 R^T(\hat{\psi}_H^{(1)}) n_\eta| \leq \begin{bmatrix} k_{21}(\bar{n}_{z_1}^{(1,1)} + \bar{n}_{z_2}^{(1,1)}) \\ k_{22}(\bar{n}_{z_1}^{(1,1)} + \bar{n}_{z_2}^{(1,1)}) \\ k_{23}(\bar{n}_z^{(1,2)}) \end{bmatrix} = \bar{\tilde{n}}_\eta$,
$| - K_2(R^T(\hat{\psi}_H^{(1)})\eta - \nu)| \leq (\tilde{\eta} - \tilde{\nu})$, with,
$|-K_2 R^T(\hat{\psi}_H)\eta| \leq \left[k_{21}(\bar{x} + \bar{y}) \ k_{22}(\bar{x} + \bar{y}) \ k_{23}(\bar{\psi})\right]^T = \tilde{\eta}, |K_2 \nu| \in \left[\underline{\nu}, \tilde{\nu}\right], \eta \in \left[\underline{\eta}, \bar{\eta}\right] \in \left[\left[\underline{x} \ \underline{y} \ \underline{\psi}\right]^T, \left[\bar{x} \ \bar{y} \ \bar{\psi}\right]^T\right]$,

and where, $\lambda_{\gamma_1^{(1)}}, \lambda_{\gamma_2^{(1)}}$ are the respective Lipschitz constants. Upon substituting the above equations into (12), $\varepsilon_{zH}^{(1)}$ satisfies

$$|\varepsilon_{zH}^{(1)}| \leq \Phi^{(1)}(t) \begin{bmatrix} \bar{p}^{(1)} \\ \bar{\psi}^{(1)} \\ \bar{\nu}^{(1)} \end{bmatrix} + \int_0^t \Bigg(\rho_d^{(1)} e^{-\xi_d^{(1)}(t-\mathfrak{t})} \begin{bmatrix} \bar{n}_z^{(1,1)} \\ \bar{n}_z^{(1,2)} \\ \mathbf{0} \end{bmatrix} + \Phi^{(1)}(t-\mathfrak{t}) \begin{bmatrix} \lambda_{\gamma_1^{(1)}} |\varepsilon_{zH}^{(1,1)}(\mathfrak{t})| \\ \lambda_{\gamma_1^{(1)}} |\varepsilon_{zH}^{(1,2)}(\mathfrak{t})| \\ \lambda_{\gamma_2^{(1)}} |\varepsilon_{zH}^{(1,3)}(\mathfrak{t})| + \bar{\tau}_e + \bar{\tilde{n}}_\eta + (\tilde{\eta} - \tilde{\nu}) \end{bmatrix} \Bigg) d\mathfrak{t}. \tag{13}$$

For $\mathcal{O}^{(2)}$, the state estimation error dynamics are given by

$$\dot{\varepsilon}_{zH}^{(2)} = \begin{bmatrix} \dot{\varepsilon}_{zH}^{(2,1)} \\ \dot{\varepsilon}_{zH}^{(2,2)} \end{bmatrix} = \begin{bmatrix} -K_3 & \mathbf{0} \\ \mathbf{0} & -K_4 \end{bmatrix} \begin{bmatrix} \varepsilon_{zH}^{(2,1)} \\ \varepsilon_{zH}^{(2,2)} \end{bmatrix} + \begin{bmatrix} \tilde{\gamma}_{1H}^{(2)} \\ \tilde{\gamma}_{2H}^{(2)} + M^{-1}\tau_e \end{bmatrix} + \begin{bmatrix} -K_3 & \mathbf{0} \\ \mathbf{0} & -K_4 \end{bmatrix} \begin{bmatrix} n_z^{(2,1)} \\ n_z^{(2,2)} \end{bmatrix}, \tag{14}$$

where, $\tilde{\gamma}_{1H}^{(2)} = r - \hat{r}_H$, and $\tilde{\gamma}_{2H}^{(2)} = M^{-1}(-C(\nu)\nu - D(\nu)\nu + C(\hat{\nu}_H^{(2)})\hat{\nu}_H^{(2)} + D(\hat{\nu}_H^{(2)})\hat{\nu}_H^{(2)})$. Similar to equation (13), a bound on the magnitude of the state estimation error under healthy conditions $|\varepsilon_{zH}^{(2)}|$ is computed, and is given by

$$|\varepsilon_{zH}^{(2)}| \leq \Phi^{(2)}(t) \begin{bmatrix} \bar{\psi}^{(2)} \\ \bar{\nu}^{(2)} \end{bmatrix} + \int_0^t \Bigg(\Phi^{(2)}(t-\mathfrak{t}) \begin{bmatrix} \lambda_{\gamma_1^{(2)}} |\varepsilon_{zH}^{(2,1)}(\mathfrak{t})| \\ \lambda_{\gamma_2^{(2)}} |\varepsilon_{zH}^{(2,2)}(\mathfrak{t})| + \bar{\tau}_e \end{bmatrix} + \rho_d^{(2)} e^{-\xi_d^{(2)}(t-\mathfrak{t})} \begin{bmatrix} \bar{n}_z^{(2,1)} \\ \bar{n}_z^{(2,2)} \end{bmatrix} \Bigg) d\mathfrak{t}, \tag{15}$$

where, $\lambda_{\gamma_1^{(2)}}$ and $\lambda_{\gamma_2^{(2)}}$ are the respective Lipschitz constants, and $|M^{-1}\tau_e| \leq \bar{\tau}_e$. Further, let us define $\rho^{(I,j)}$, $\xi^{(I,j)}$, $\rho_d^{(I,j)}$, $\xi_d^{(I,j)}$ as positive constants satisfying $|e^{-K_p t}| \leq \rho^{(I)} e^{-\xi^{(I)} t}$ and $\xi^{(I)} > \Lambda_I \rho^{(I)}$, $p \in \{1, \ldots, 4\}$; $\Lambda_1 = \lambda_{\gamma_1^{(1)}}$, $\Lambda_2 = \begin{bmatrix} \lambda_{\gamma_1^{(2)}} & \mathbf{0} \\ \mathbf{0} & \lambda_{\gamma_2^{(2)}} + \lambda_{\bar{\tau}_e} \end{bmatrix}$. Applying the Bellman-Gronwall lemma to equations (13), (15), and by using the relation in (9), the $j-$th component of the adaptive threshold ($j \in \{1,2\}$) for the sensor faults in $\mathcal{S}^{(1)}$ can be expressed as (Reppa et al. (2016))

$$\begin{aligned} \bar{\varepsilon}_{y_z}^{(1,j)}(t) =& E^{(1,j)}(t) + \rho^{(1,j)} \Lambda_1 \int_0^t Z^{(1,j)}(\mathfrak{t}) e^{-\xi^{(1,j)}(t-\mathfrak{t})} d\mathfrak{t} \\ &+ \bar{n}_z^{(1,j)}, \quad \text{where,} \end{aligned} \tag{16}$$

$$\begin{aligned} E^{(1)}(t) =& \rho^{(1)} e^{-\xi^{(1)} t} \bar{z}^{(1)} + \frac{\rho_d^{(1)} \bar{n}_z^{(1)}}{\xi_d^{(1)}} (1 - e^{-\xi_d^{(1)} t}) \\ &+ \int_0^t \rho^{(1)} e^{-\xi^{(1)}(t-\mathfrak{t})} \begin{bmatrix} \mathbf{0} \\ \bar{\tau}_e + \bar{\tilde{n}}_\eta + (\tilde{\eta} - \tilde{\nu}) \end{bmatrix} d\mathfrak{t}, \\ Z^{(1)}(t) =& E^{(1)}(t) + \rho^{(1)} \Lambda_1 \int_0^t E^{(1)}(\mathfrak{t}) e^{(\rho^{(1)}\Lambda_1 - \xi^{(1)})(t-\mathfrak{t})} d\mathfrak{t}. \end{aligned} \tag{17}$$

Similarly, for the faults occurring in the sensor set $\mathcal{S}^{(2)}$, the $j-$th adaptive threshold ($j \in \{1,2\}$) is expressed as

$$\begin{aligned} \bar{\varepsilon}_{y_z}^{(2,j)}(t) =& E^{(2,j)}(t) + \rho^{(2,j)} \Lambda_2^{(j)} \int_0^t Z^{(2,j)}(\mathfrak{t}) e^{-\xi^{(2,j)}(t-\mathfrak{t})} d\mathfrak{t} \\ &+ \bar{n}_z^{(2,j)}, \quad \text{where,} \end{aligned} \tag{18}$$

$$\begin{aligned} E^{(2)}(t) =& \rho^{(2)} e^{-\xi^{(2)} t} \bar{z}^{(2)} + \frac{\rho_d^{(2)} \bar{n}_z^{(2)}}{\xi_d^{(2)}} (1 - e^{-\xi_d^{(2)} t}) \\ &+ \int_0^t \rho^{(2)} e^{-\xi^{(2)}(t-\mathfrak{t})} \begin{bmatrix} 0 \\ \bar{\tau}_e \end{bmatrix} d\mathfrak{t}, \\ Z^{(2)}(t) =& E^{(2)}(t) + \rho^{(2)} \Lambda_2 \int_0^t E^{(2)}(\mathfrak{t}) e^{(\rho^{(2)}\Lambda_2 - \xi^{(2)})(t-\mathfrak{t})} d\mathfrak{t}. \end{aligned} \tag{19}$$

Remark 1. Under the absence of noise and unknown disturbances, asymptotic convergence of the state estimation error to zero can be ensured by selecting the observer gains K_1, K_2 and K_4 as positive definite matrices, and $K_3 > 0$.

3.3 Combinatorial Fault Decision Logic

To diagnose multiple sensor faults, a combinatorial fault decision logic is designed. Firstly, a decision on the detection of a fault is obtained based on a set of ARRs of residuals and adaptive thresholds. For the monitoring module $\mathcal{M}^{(I)}$, the set of ARRs $\mathcal{E}_{y_z}^{(I)}$ are defined for detecting faults in the sensor set $\mathcal{S}^{(I)}$, as $\mathcal{E}_{y_z}^{(I)} = \bigcup_j \mathcal{E}_{y_z}^{(I,j)}$, where, for $I \in \{1, 2\}$, the $j-$th ARR $\mathcal{E}_{y_z}^{(I,j)}$ is given by

$$\begin{aligned} \mathcal{E}_{y_z}^{(1,j)} &: |\varepsilon_{y_z}^{(1,j)}(t)| - \bar{\varepsilon}_{y_z}^{(1,j)}(t) \leq 0, \quad j \in \{1, 2\}, \\ \mathcal{E}_{y_z}^{(2,j)} &: |\varepsilon_{y_z}^{(2,j)}(t)| - \bar{\varepsilon}_{y_z}^{(2,j)}(t) \leq 0, \quad j \in \{1, 2\}. \end{aligned} \tag{20}$$

A violation of the $j-$th ARR implies the occurrence of at least one sensor fault in the corresponding sensor set $\mathcal{S}^{(I)}$. Let define $T_D^{(I,j)}$ to be the first instance of violation of the $j-$th ARR $\mathcal{E}_{y_z}^{(I,j)}$ in $\mathcal{M}^{(I)}$, i.e.,

$$T_D^{(I,j)} = \min\{t : |\varepsilon_{y_z}^{(I,j)}(t)| > \bar{\varepsilon}_{y_z}^{(I,j)}(t)\}. \tag{21}$$

If $\mathcal{E}_{y_z}^{(I,j)}$ is always satisfied, then $T_D^{(I,j)}$ is taken to be infinity. The fault detection time for module $\mathcal{M}^{(I)}$ is defined as $T_{FD}^{(I)} = \min_t\{T_D^{(I,j)}, \forall j\}$. The output of the monitoring module $\mathcal{M}^{(I)}$ is the $I-$th decision $D^{(I)}(t) = \left[D^{(I,1)}(t),\ \ldots,\ D^{(I,m_I)}(t)\right]^T$, where,

$$D^{(I,j)}(t) = \begin{cases} 0, & \text{if } t < T_D^{(I,j)} \\ 1, & \text{otherwise} \end{cases}. \tag{22}$$

Under the exoneration assumption (Reppa et al. (2013)) which considers that $\mathcal{S}^{(I)}$ is functioning properly before the time instant $T_{FD}^{(I)}$, $D^{(I)}(t) = \mathbf{0}$ implies that no fault has occurred in the sensor set $S^{(I)}$.

Upon obtaining the decisions $D^{(I)}(t)$ from each monitoring module, fault isolation is performed by combining the decisions in the aggregator module $\mathcal{A}$ into a decision vector $D(t)$. Thereafter, a consistency test is performed between $D(t)$ and a binary fault signature matrix (FSM) F. F consists of l rows, $l = \sum_I m_I$, with each row corresponding to the $j-$th ARR $\mathcal{E}_{y_z}^{(I,j)}$, and $N_c = 2^{\mathfrak{s}} - 1$ columns, where $\mathfrak{s}$ is the total no. of monitored sensors. The $q-$th column F_q, $q \in \{1, \ldots, N_c\}$ is referred to as a theoretical sensor fault pattern, and $F_{pq} = 1$ ($p \in \{1, \ldots, l\}$), suggests that at least one sensor fault included in the combination $\mathcal{F}_{c_q}$ is responsible for the violation of the ARR $\mathcal{E}_{y_z}^{(I,j)}$, and therefore, affects $\mathcal{S}^{(I)}$. F_{pq} = " $*$ " is used instead of "1" to distinguish a possible violation due to the weak sensitivity of the ARR $\mathcal{E}_{y_z}^{(I,j)}$ to a sensor fault included in $\mathcal{F}_{c_q}$. Otherwise, F_{pq} is taken to be zero. The observed fault pattern in $D(t)$ is said to be consistent with the theoretical pattern in F_q when $D_p(t) = F_{pq}$, $\forall p \in \{1, \ldots, l\}$. Finally, the diagnosis set $D_s(t)$ is obtained as the output of the aggregator, which consists of all the possible fault combinations $\mathcal{F}_{c_q}$, obtained as a result of the consistency test. Note that as the elements of $D(t)$ vary over time, the cardinality of the diagnosis set may also change.

4. SIMULATION RESULTS

In this section, a simulation study is presented with a vessel tracking a predefined trajectory to evaluate the effectiveness of the proposed FDI approach. A model vessel named "*Tito-Neri*", which is developed at TU Delft, is considered and represents a 1:30 replica of a harbour tug. Its hydrodynamic model parameters are provided in Bruggink et al. (2018). The wind is modeled in this simulation at a velocity of $V = 2$ m/s and an angle of $\beta_V = 45$ degrees, coming from the southwest direction. Further, the damping force $D(\nu)\nu$ is not considered as in the vessel model equations (1), instead, it is modelled as a drag vector, which is obtained through experiments and mathematical approximations. In this work, the drag vector is taken as the unknown force vector τ_d. Finally, $\bar{\tau}_e$ is taken to be equal to $M^{-1}(|\tau_w| + 1.05 \times |\tau_d|)$.

The simulation is carried out for a total duration of 3000 seconds. The fault detection observer gain matrices K_1, K_2, K_4 are taken to be equal to a diagonal matrix diag([100, 100, 100]), and K_3 is equal to 100. Each sensor is assumed to be corrupted by Gaussian white noise having an amplitude within 3% of the mean absolute value of the noiseless sensor measurement. Further, the design parameters for the adaptive thresholds in each of the monitoring modules are selected as follows: $\rho^{(1,1)} = \rho^{(1,2)} = \rho^{(2,1)} = 0.001; \xi^{(1,1)} = \xi^{(1,2)} = \xi^{(2,1)} = 1; \rho_d^{(1,1)} = \rho_d^{(1,2)} = \rho_d^{(2,1)} = 10; \xi_d^{(1,1)} = \xi_d^{(1,2)} = \xi_d^{(2,1)} = 1; \rho^{(2,2)} = 1, \xi^{(2,2)} = 95, \rho_d^{(2,2)} = 0.1, \xi_d^{(2,2)} = 4$. The theoretical fault signatures used in the aggregator module are provided in Table 1, where, $\mathcal{F}_{c_1} = \{f_p\}$, $\mathcal{F}_{c_2} = \{f_\psi\}$, $\mathcal{F}_{c_3} = \{f_\nu\}$, $\mathcal{F}_{c_4} = \{f_p, f_\psi\}$, $\mathcal{F}_{c_5} = \{f_p, f_\nu\}$, $\mathcal{F}_{c_6} = \{f_\psi, f_\nu\}$ and $\mathcal{F}_{c_7} = \{f_p, f_\psi, f_\nu\}$. Given the structure of the FSM matrix, it is clear that any combination of faults can be isolated, which can be further verified by simulating different fault scenarios.

Table 1. Sensor fault signature matrix for the aggregator $\mathcal{A}$

	$\mathcal{F}_{c_1}$	$\mathcal{F}_{c_2}$	$\mathcal{F}_{c_3}$	$\mathcal{F}_{c_4}$	$\mathcal{F}_{c_5}$	$\mathcal{F}_{c_6}$	$\mathcal{F}_{c_7}$
$\mathcal{E}_{y_z}^{(1,1)}$	1	*	0	1	1	*	1
$\mathcal{E}_{y_z}^{(1,2)}$	0	1	0	1	0	1	1
$\mathcal{E}_{y_z}^{(2,1)}$	0	1	1	1	1	1	1
$\mathcal{E}_{y_z}^{(2,2)}$	0	0	1	0	1	1	1

As a fault scenario, permanent faults in the gyrocompass and GPS/GNSS sensors are considered to have occurred at $T_{f_\psi} = 500$ sec and $T_{f_p} = 1500$ sec, respectively. The respective fault functions are given by $f_\psi = u(t - T_{f_\psi})(A_{f_\psi} + (1 - e^{-(t-T_{f_\psi})}))$, $f_p = u(t - T_{f_p})(A_{f_p} + \sin(0.45t))$, where $u(t)$ denotes a unit step function, and, A_{f_ψ}, A_{f_p} are fault amplitudes ranging between $1-2$ times the mean absolute values of the noiseless sensor measurement. The resulting residual signals and the corresponding adaptive thresholds for the j^{th} sensor monitored by $\mathcal{M}^{(I)}$ are plotted under $\mathcal{M}^{(I,j)}$ in Figure 2. As shown, the residuals corresponding to the gyrocompass (in $\mathcal{M}^{(1,2)}$ and $\mathcal{M}^{(2,1)}$) exceed the thresholds at $t = 500$ secs, whereas, the residuals corresponding to the GPS/GNSS (in $\mathcal{M}^{(1,1)}$) exceed the thresholds at $t = 1500$ secs. For $t < 500$ secs, the components of

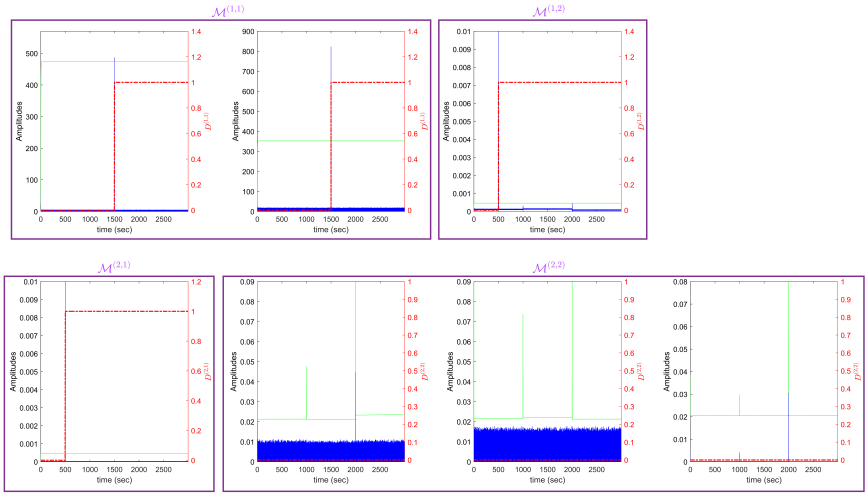

Fig. 2. Simulation results of the residual signals, the corresponding adaptive thresholds, and the decision vectors for each monitoring module

the detection vectors $D(t)$ remain zero, and the diagnosis set corresponds to a null set. For $500 \leq t < 1500$ secs, the occurrence of the first fault is detected by the residual exceeding the adaptive threshold, which results in $D(t) = [0\ 1\ 1\ 0]^T$. For $t \geq 1500$ sec, the second fault is detected, leading to $D(t) = [1\ 1\ 1\ 0]$. At the end of the simulation, a consistency test is performed by comparing the observed pattern $D(t)$ to the theoretical patterns $\mathcal{F}_{c_q}$, which results in a diagnosis set $\mathcal{D}_s(t) = \{\mathcal{F}_{c_2}, \mathcal{F}_{c_4}\} = \{\{f_\psi\}, \{f_p, f_\psi\}\}$, thereby isolating the faulty sensors.

5. CONCLUSIONS

In this paper, we propose an observer-based FDI scheme for diagnosing multiple faults occurring in the navigational sensors of an ASV. The proposed FDI scheme employs various monitoring modules to diagnose the respective sensor sets using a bank of nonlinear observer-based residuals and thresholds that are structurally sensitive to faults. Additionally, an aggregator module that is integrated with a combinatorial fault decision logic facilitates the isolation of the faulty sensors. Finally, we also obtained adaptive thresholds for bounding the residual signals, thereby ensuring that no false alarms occur. As demonstrated through the simulations, the proposed technique is capable of isolating the possible combinations of faults occurring in the considered set of navigational sensors. A limitation of the proposed method is that delays in the violation of ARRs on the occurrence of fault combinations could lead to inaccurate fault isolation. This problem can be resolved by considering the sensitivity of ARRs to various faults during the design of the FSM, which is proposed for future work.

REFERENCES

Blanke, M. (2006). Fault-tolerant sensor fusion for marine navigation. In *7th IFAC Conference on Maneuvering and Control of Marine Craft*, 1385–1390. Elsevier.

Bruggink, D., Cremer, Q., Groenewegen, R., and Klokgieters, A. (2018). Differentiation of maneuvering coefficients for scaled model vessels. Technical report, Delft University of Technology.

Fossen, T.I. (2011). *Handbook of marine craft hydrodynamics and motion control*. John Wiley & Sons.

Kepaptsoglou, K., Fountas, G., and Karlaftis, M.G. (2015). Weather impact on containership routing in closed seas: A chance-constraint optimization approach. *Transportation Research Part C: Emerging Technologies*, 55, 139–155.

Lin, Y., Du, J., Zhu, G., and Fang, H. (2018). Thruster fault-tolerant control for dynamic positioning of vessels. *Applied Ocean Research*, 80, 118–124.

Liu, Z., Zhang, Y., Yu, X., and Yuan, C. (2016). Unmanned surface vehicles: An overview of developments and challenges. *Annual Reviews in Control*, 41, 71–93.

Park, B.S. and Yoo, S.J. (2016). Fault detection and accommodation of saturated actuators for underactuated surface vessels in the presence of nonlinear uncertainties. *Nonlinear Dynamics*, 85(2), 1067–1077.

Reppa, V., Polycarpou, M.M., and Panayiotou, C.G. (2013). Adaptive approximation for multiple sensor fault detection and isolation of nonlinear uncertain systems. *IEEE Transactions on Neural Networks and Learning Systems*, 25(1), 137–153.

Reppa, V., Polycarpou, M.M., Panayiotou, C.G., et al. (2016). Sensor fault diagnosis. *Foundations and Trends® in Systems and Control*, 3(1-2), 1–248.

Rogne, R.H., Johansen, T.A., and Fossen, T.I. (2014). Observer and imu-based detection and isolation of faults in position reference systems and gyrocompasses with dual redundancy in dynamic positioning. In *2014 IEEE Conference on Control Applications (CCA)*, 83–88. IEEE.

Wang, N., Pan, X., and Su, S.F. (2020). Finite-time fault-tolerant trajectory tracking control of an autonomous surface vehicle. *Journal of the Franklin Institute*, 357(16), 11114–11135.

Zhang, Q., Zhang, X., Zhu, B., and Reppa, V. (2021). Fault tolerant control for autonomous surface vehicles via model reference reinforcement learning. In *2021 60th IEEE Conference on Decision and Control (CDC)*, 1536–1541. IEEE.